Journal of ELECTRONIC MATERIALS, Vol. 50, No. 4, 2021
https://doi.org/10.1007/s11664-020-08568-y

ASIAN CONSORTIUM ACCMS–INTERNATIONAL CONFERENCE ICMG 2020

Inter-relationship of the Structural Properties of Quaternary Chalcogenides $CuZn_2Ga(S/Se)_4$: A First-Principles Study

M.V. JYOTHIRMAI [1,2,3]

1.—SRM Research Institute, SRM Institute of Science and Technology, Kattankulathur, Tamil Nadu 603203, India. 2.—Department of Physics, SRM University-AP, Amaravati, Andhra Pradesh 522502, India. 3.—e-mail: mvmjyothi@gmail.com

Quaternary chalcogenides based on stannite I-II_2-III-VI_4 structure are the best potential candidates to overcome the current generation of solar harvesting materials. First-principles electronic structure simulations were performed on semiconducting $CuZn_2Ga(S/Se)_4$ (CZGS/Se) to understand the inter-relationship of the structural properties. These structures contain a cubic close packing (ccp) array of S/Se-centered tetrahedrons, coordinated by one Cu, two Zn and one Ga atom occupying one half of the ccp tetrahedral voids. The remarkable variations in the crystal structures are explained by the influence of ionic radii of various atoms. The electronic and optical properties calculated using hybrid functional (Heyd, Scuseria and Ernzerhof, HSE06) show a suitable band gap of 1.59 eV for CZGSe with high optical absorption. The current density and maximum upper limit of theoretical energy conversion efficiency ($P(\%)$) of CZGSe is enhanced when compared to that of CZGS. Our results suggest that the stannite CZGSe structure could be a promising candidate for efficient earth-abundant thin-film solar cell applications.

Key words: Solar absorber materials, $CuZn_2Ga(S/Se)_4$, first-principles calculations, electronic band structure, performance characteristics

INTRODUCTION

The relentless demand for solar energy harvesting has motivated the scientific community to design stable and better performing photovoltaic materials.[1–5] In this regard, multicomponent chalcogenides with tremendous diversity and remarkable flexibility of spatial arrangements are considered as potential candidates for various industrial and scientific applications, including transport, magnetism and optoelectronics. Such materials can modify the physicochemical properties through cation mutations to meet the needs for future generations.[6] Particularly, from binary II-VI wurtzite or zinc-blende material, one can generate I-III-VI_2 ternary or I_2-II-IV-VI_4/I-II_2-III-VI_4 quaternary compounds (I = Cu, Ag; II = V, Fe, Co, Ta, Zn, Cd; III = Al, Ga, In, Tl; IV = Si, Ge, Sn; VI = S, Se, Te). In addition, the composition of eco-friendly and earth-abundant constituents make these multicomponent chalcogenides more advantageous and attractive for designing ecologically clean and cost effective devices for solar energy-conversion applications.[7–10] This approach tunes the electronic band gap of a system into a convenient solar absorption region and thus enhances their suitability for photovoltaic cells. Specifically, $Cu_2ZnSn(S/Se)_4$[11–14] has gathered immense interest in solar cell and photovoltaic applications because of its tunable electronic (1.0–1.5 eV)[15–17] and optical (10^4 cm^{-1})[17,18] properties. However, these quaternary chalcogenides show low power conversion efficiencies when compared with other thin-film solar cells. Therefore, a novel class of I_2-II-IV-VI_4/I-II_2-III-VI_4 chemical compositions must

(Received September 10, 2020; accepted October 15, 2020; published online November 9, 2020)

be determined from ternary I-III-VI_2 structures to overcome performance limitations.

Unlike quaternary I_2-II-IV-VI_4, the semiconducting chalcogenides I-II_2-III-VI_4 are practically unexplored and few experimental and theoretical studies are reported to understand the physicochemical properties of these materials. For instance, it has been shown that $AgZn_2InTe_4$, $CuCd_2InTe_4$, $CuZn_2InTe_4$ and $CuTa_2InTe_4$ can be synthesized by modifying the cubic lattice structures or tetragonal stannite (ST) and possess relatively low thermal conductivity.[19–22] Density functional theory (DFT) calculations were performed on a series of stannite $CuFe_2$-III-VI_4 (III= Al, Ga, In and VI = S, Se and Te) and it was found that the band gap value increases as the anion atomic number decreases while keeping the cation unchanged.[23] Specifically, $CuZn_2GaS/Se_4$ (CZGS/Se) materials have garnered much interest because of the ambiguity in their valence states together with iso-electronic nature of their constituent atoms (Cu = 29, Zn = 30, Ga = 31). Yalcin et al.[24] studied the physicochemical properties of semiconducting chalcogenides $CuZn_2AS_4$ (CZAS; A = Al, Ga and In) and they found that the stannite phase as an energetically stable structure. These materials exhibit appropriate band gap values (0.81–1.71 eV) with a high absorption cross section, which makes them suitable candidates for solar harvesting applications. Bindi et al.[25] synthesized tetragonal structure of stannite phase $CuZn_2GaS_4$ quaternary chalcogenide. The crystal structure is composed of alternating layers of II-VI atoms and I-III atoms arranged along the vertical direction. Recently, Wencong et al. performed electronic structure calculations for a series of 36 possible I-II_2-III-VI_4 (I = Cu, Ag; II = Zn, Cd; III = Al, Ga, In; VI = S, Se, Te) chemical compositions and found that these chalcogenides range from semiconductor to semimetal based on the phase and chemical compositions.[10]

Here, first-principles calculations were performed to investigate the inter-relationship of the structural properties of stannite quaternary chalcogenides CZGS/Se. The remarkable changes in the crystal structure of quaternary chalcogenides were explained quantitatively. The electronic and optical properties using sate-of-the-art hybrid functionals show suitable band gaps with high absorption coefficients. To estimate the performance of these materials, we have calculated the current density and maximum upper limit of theoretical energy conversion efficiency (P(%)). The present work manifests the importance of CZGS/Se materials for producing high performance light-to-electricity conversion in photovoltaic devices.

COMPUTATIONAL METHODS

The quaternary chalcogenides $CuZn_2Ga(S/Se)_4$ were studied using the Vienna Ab initio Simulation Package (VASP)[26,27] via projector-augmented wave (PAW)[28] approach within the framework of density functional theory (DFT). The generalized gradient approximation (GGA) is considered to include the effects of exchange-correlation (XC) functional through Perdew–Burke–Ernzerhof (PBE) parameterization.[29] The structural optimization was performed using a conjugate-gradient algorithm with a plane-wave kinetic energy cutoff and energy convergence criterion of 500 eV and 10^{-5} eV, respectively. The relaxation was conducted until the forces on each atom were diminished to 0.01 eV/Å. The Monkhorst-Pack grid scheme[30] is employed to generate a suitable k-point grid of $7 \times 7 \times 5$. In order to account for the derivative discontinuity in the exchange-correlation functional as well as to overcome the self-interaction error generally observed in the standard DFT functionals (eg. LDA and GGA),[31–36] we adopted the Heyd–Scuseria–Ernzerhof 06 (HSE06) hybrid functional[37,38] to produce appropriate band gap values. In this approach, a nonlocal Hartree–Fock (HF) exchange energy of 25% (a = 0.25) is used with the PBE scheme with a screening parameter of v = 0.2 $Å^{-1}$. For HSE calculations , the Γ centred k-point mesh is used to study the electronic and optical properties.

$$E_{XC}^{HSE} = \alpha E_X^{HF,SR}(\mu) + (1-\alpha)E_X^{PBE,SR}(\mu) + E_X^{PBE,LR}(\mu) + E_C^{PBE} \quad (1)$$

Here, the exchange energy (E_X^{HSE}) in the HSE functional is divided into long-range (LR) and short-range (SR) components: the LR portion has only a PBE term ($E_X^{PBE,LR}$), while the SR portion contains both HF ($E_X^{HF,SR}$) and PBE ($E_X^{PBE,SR}$) terms.

STRUCTURAL PROPERTIES

The stannite CZGS/Se crystallizes in the tetragonal structure with space group I-42 m. This chalcopyrite structure obeys the octet rule, which is characterized by the coordination of the chalcogen atoms group by the I and III atomic groups. It contains 16 atoms in the conventional tetragonal body-centered unit cell, while the body-centered primitive unit cell contains eight atoms. The crystal structure of stannite CZGS/Se along different crystallographic directions is depicted in Fig. 1. Here, the Cu and Ga atoms occupy 2b (0,0,1/2) and 2a (0, 0, 0) Wyckoff sites, respectively. The Zn atoms are located at 4d (0,1/2,1/4) sites, while group VI (S/Se) atoms reside in the 8i (x, y, z) sites. The layers at z = 1/4 and 3/4 have only Cu atoms. The packing of S/Se atoms are found to deviate slightly from the ideal position due to the presence of Ga atoms. Further, the structure possess cubic close packing (ccp) array of S/Se-centered tetrahedral, which is coordinated by one Cu, two Zn and one Ga atoms occupying one half of the ccp tetrahedral voids.

Initially, the quaternary CZGS/Se structures are fully relaxed using PBE-GGA functional and the obtained lattice parameter, volume, bond lengths

and band gaps are presented in Table I. For the CZGS structure, the lattice constants $a = b = 5.42$ Å and $c = 10.76$ Å are in accord with the reference values of 5.36 Å and 10.58 Å,[25] respectively, while the lattice parameters for CZGSe structure are found to be $a = b = 5.72$ Å and $c = 11.35$ Å. The $a = b$ value of CZGSe increases by 5.53% as compared to CZGS, while the relative increase in c is 5.48%. The corresponding volume of CZGSe is increased by 17.23%. The overall enhancement in the equilibrium lattice constants and volume by replacing the group VI atoms with higher atomic number is due to the larger size of selenium when compared with that of the S atom. Further, the remarkable variations in the crystal structures can be explained by understanding the influence of ionic radii of various atoms. Particularly, we compare the Cu-S/Se, Zn-S/Se and Ga-S/Se atomic distances for both the CZGS and CZGSe structures. The small ionic radius of S (~ 1.84 Å) together with the ionic radius of Cu (~ 0.73 Å), Zn(~ 0.74 Å) and Ga (~ 0.62 Å) results in Cu-S, Zn-S and Ga-S bond lengths of 2.32, 2.36 and 2.33 Å, while the larger ionic radius of Se (~ 1.98 Å) yields a bigger Cu-Se, Zn-Se and Ga-Se bond lengths of 2.44 Å, 2.49 Å and 2.47 Å, respectively. This anisotropic behavior among the structure of CZGS and CZGSe also varies the distance between S(Se) and S(Se) atoms of two adjacent layers along c-direction (3.86/4.06 Å).

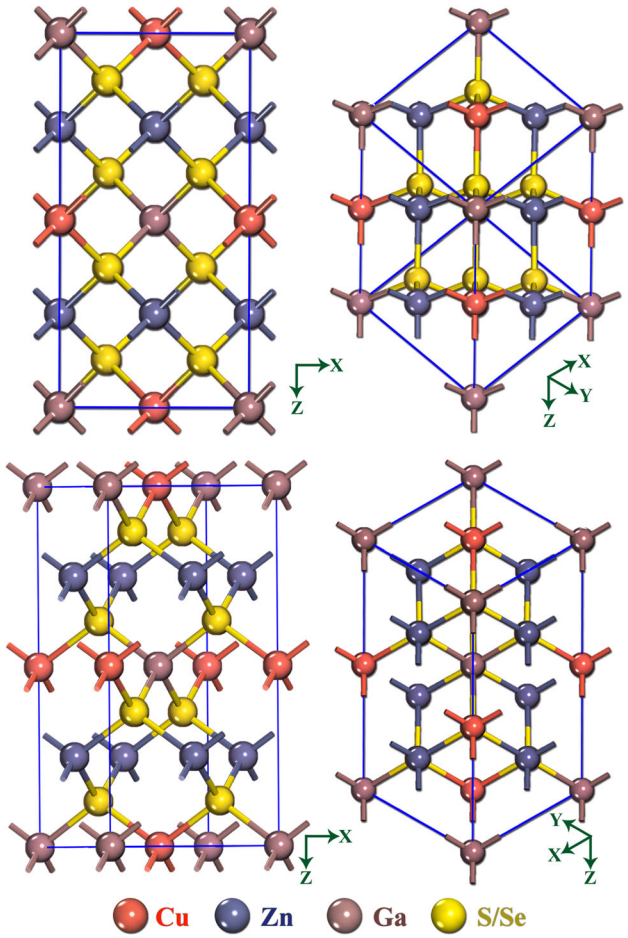

Fig. 1. Crystal structure of CZGS/Se along various crystallographic directions.

ELECTRONIC PROPERTIES

Most of the quaternary chalcogenides are semiconducting materials, and thus the prediction of accurate band gap values are very crucial in understanding the solar cell performance. Generally, the absence of quasi-particle excitations in the standard DFT functionals (e.g. LDA and GGA) hinders the inherent promising features. To overcome this problem, the Heyd–Scuseria–Ernzerhof (HSE 06) hybrid functional is used to calculate the electronic and optical properties, which brings the electronic band gaps close to the measured values. The electronic band structure of stannite CZGS/Se within the HSE functional is plotted in Fig. 2. Both the band structures are almost identical due to their similar geometric configurations. It is clearly seen from the figure that both structures are semiconductors with direct band gap; i.e., the valence band maximum (VBM) and conduction band minimum (CBM) lies on the same Γ-point. The calculated band gap values of CZGS and CZGSe using the PBE-GGA functional is found to be 1.13 eV and 0.45 eV, respectively. Even though the standard DFT functional provides a preferred curvature of the bands, it severely underestimates the electronic band gap

Table I. Calculated lattice parameters, volume, bond length and band gap of $CuZn_2GaS_4$ and $CuZn_2GaSe_4$

		$CuZn_2GaS_4$	$CuZn_2GaSe_4$
Lattice parameters (Å)	a	5.42	5.72
	c	10.76	11.35
Bond length (Å)		Cu-S: 2.32	Cu-Se: 2.44
		Zn-S: 2.36	Zn-Se: 2.49
		Ga-S: 2.33	Ga-Se: 2.47
Volume (Å^3)		316.48	371.03
Band gap (eV)	PBE	1.13	0.45
	HSE	2.41	1.59

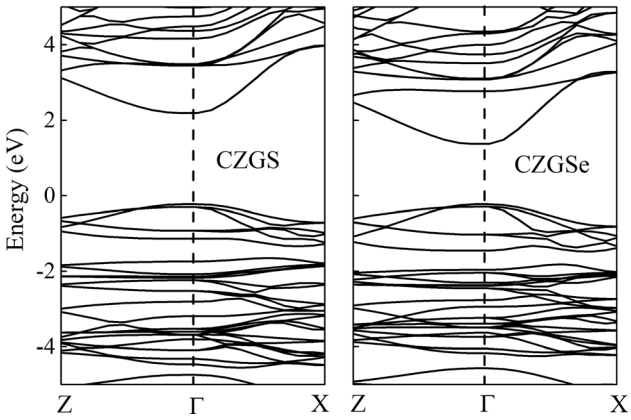

Fig. 2. The calculated band structure of stannite CZGS and CZGSe using HSE06 functional.

values. On the other hand, the HSE functional produces improvised band gap values of 2.41 eV and 1.59 eV for CZGS and CZGSe, respectively. The relative band gap decrease of CZGSe is mainly due to the downshift of conduction bands, likely related to an increase in the corresponding ionic radius of the Se atom. Yalcin[24] calculated the electronic band structure of $CuZn_2GaS_4$ using a modified Becke-Johnson (mBJ) potential and found the band gap of 2.02 eV, which is 16.1% less than our HSE value.

The total and partial density of states (TDOS/PDOS) are also calculated to understand the effect of atomic relaxation and the bonding situation on the electronic band structure. Figure 3 represents the partial/total density of states (PDOS/TDOS) of CZGS/Se using HSE functional along high symmetry directions in the first Brillouin zone. For CZGS, the Fermi level near the valence range is mainly derived from S atoms, while the CBM is dominated by Ga and S atoms. In the case of CZGSe, the CBM is clearly made up of Ga and Se atoms, although there are some minor contributions from Cu and Zn atoms. The VBM, on the other hand, is mainly derived from Cu and Se atoms. For both the cases, a sizeable hybridization is observed between Cu and Se atoms in the energy range of − 1 eV. The S-Ga hybridization is stronger than Se-Ga due to the shorter S-Ga bond lengths, thereby the CBM is slightly shifted downwards.

OPTICAL PROPERTIES

The copper-based quaternary chalcogenides are potential candidates for optoelectronic applications because they are direct band gap semiconductors. Typically, the complex dielectric function is mainly responsible for optical parameters of solids: $\epsilon(\omega) = \epsilon_1(\omega) + i\epsilon_2(\omega)$, where $\epsilon_1(\omega)$ and $\epsilon_2(\omega)$ denotes the real and imaginary parts of the dielectric function. The dielectric functions of CZGS/Se structures contain two components $\epsilon_{xx}(\omega)$ and $\epsilon_{zz}(\omega)$, which corresponds to the polarization along x/y and z directions. The calculated real $\epsilon_1(\omega)$ and imaginary $\epsilon_2(\omega)$ parts and absorption coefficient as functions of photon energy

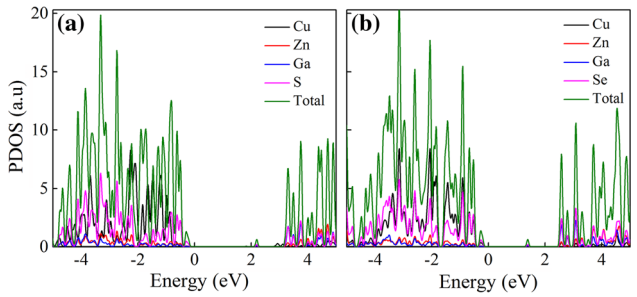

Fig. 3. Calculated total and partial density of states (TDOS/PDOS) of stannite (a) CZGS and (b) CZGSe using HSE06 functional.

for CZGS/Se structures are shown in Fig. 4a, b, c, d, e, and f. The static dielectric constant, $\epsilon_1(0)$, can be used to understand the electric polarizability of a material and it is the value where the real part $\epsilon_1(\omega)$ interacts with the vertical axis. Here the static dielectric constant of CZGS and CZGSe is found to be 5.66 and 7.31, respectively. It should be noted that the smaller band gaps produces larger value of $\epsilon_1(0)$. This inverse behavior is related to Penn's model: $\epsilon_1(0) \approx 1 + (\hbar\omega_p/E_g)^2$,[39] where E_g and ω_p correspond to energy band gap and plasma frequency, respectively. The strong peaks in the real part are observed at 5.25 eV and 3.3 eV for CZGS and CZGSe, respectively, where the energy numbers of CZGSe belong to the visible region of the electromagnetic spectrum. Moreover, the most pronounced peak of CZGSe is enhanced when compared to that of CZGS. The negative values are also observed in the real part around 7.6–18.5 eV, which represents that the incident photons are completely reflected in this region.

The transitions between the occupied and unoccupied bands can be described using imaginary part, $\epsilon_2(\omega)$, of the dielectric function. The fundamental absorption edge from the $\epsilon_2(\omega)$ is observed at 2.26 eV and 1.45 eV for CZGS and CZGSe, respectively, which is in accord with the observed band gap values and also confirms the direct optical transition along theΓ point between VBM and CBM. Further, the peak in the visible region is much more pronounced for CZGSe, which indicates high solar absorbance capability of the material. The absorption coefficient is an important optical constant to understand the light absorption behavior of a material. The absorption coefficient is zero until the energy of 1.19 eV and 0.6 eV for CZGS and CZGSe, respectively, and thereby increases, indicating the absorption of light from that particular photon energy. The maximum absorption peak of 0.84×10^5 cm^{-1} and 1.18×10^5 cm^{-1} for CZGS and CZGSe is observed in the visible region at 2.6 eV and 1.75 eV, while the strongest absorption in the spectrum is observed at 4.0 eV and 3.4 eV, respectively. These semiconducting chalcogenides with high absorption coefficient in the visible region of

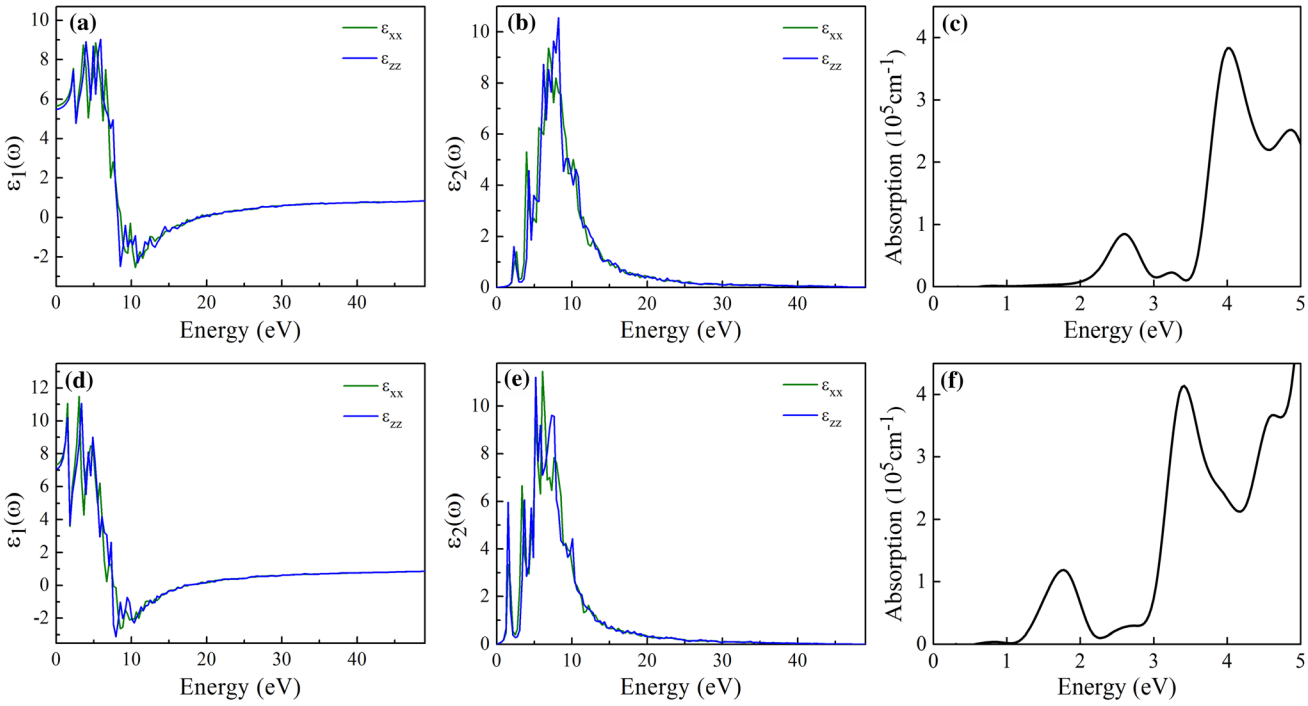

Fig. 4. Calculated (a and d) real part $\epsilon_1(\omega)$ (b and e) imaginary part $\epsilon_2(\omega)$ of dielectric function and (c and f) absorption coefficient of CZGS and CZGSe, respectively.

$> 10^5$ represents their importance in solar harvesting applications.

PERFORMANCE PROPERTIES

The current density and maximum upper limit of theoretical energy conversion efficiency ($P(\%)$) is very important to understand the efficiency of solar absorber materials. The overlap between solar spectrum and absorbance can provide the theoretical power conversion efficiency ($P(\%)$):

$$P = \int_0^{\lambda_{max}} W(\lambda)A(\lambda)C(\lambda)d\lambda \int_0^{\infty} W(\lambda)d\lambda \qquad (2)$$

where λ, $W(\lambda)$ and λ_{max} represent photon wavelength, solar spectral irradiance and the longest wavelength that can be absorbed by the system, respectively. The energy band gap (E_g) can be used to estimate the λ_{max} :

$$\lambda_{max} = hcE_g \qquad (3)$$

The conversion factor $C(\lambda)$ and the absorbance $A(\lambda)$ are calculated using the following equation:

$$C(\lambda) = \lambda \frac{E_g}{hc} \qquad (4)$$

$$A(\lambda) = 1 - e^{-\alpha(\lambda)d} \qquad (5)$$

where E_g, d and α denote the minimum band gap, thickness and the absorption coefficient of the material, respectively. The absorbed photon flux J_{abs} was calculated using the following equation under Air Mass 1.5 G solar illumination:

$$J_{abs} = e \int_{E_g}^{\infty} A(E)J_{ph}(E)dE \qquad (6)$$

Here J_{ph}, E, E_g and A represents the incident photon flux, photon energy, band gap and the absorbance, respectively.

The calculated electronic band gap, current density and energy conversion efficiency P (%) of CZGS is found to be 2.41 eV, 4.8 mA/cm^2 and 4.11% respectively, while CZGSe has a band gap of 1.59 eV, current density of about 15.8 mA/cm^2 and P of 11.4%. This clearly indicates that the CZGSe contains significantly high P (%) compared to CZGS and may be related to the corresponding band gaps, where the smaller band gap of CZGSe produces enhanced photocurrent density and energy conversion efficiency.

CONCLUSIONS

In summary, we present the inter-relationship of structural properties of quaternary stannite chalcogenides CZGS/Se using first-principles calculations. The packing of S/Se atoms in the crystal structures of CZGS/Se are found to deviate slightly from the ideal position due to the presence of Ga atoms. The electronic band structure using the HSE functional demonstrates that these materials are semiconductors with a direct band gap of 2.41 eV and 1.59 eV for CZGS and CZGSe, respectively, and the decrease in the bandwidth for the latter is mainly due to an

increase in the ionic radius of the corresponding Se atom. The maximum absorption of 0.84×10^5 cm^{-1} and 1.18×10^5 cm^{-1} is observed for CZGS and CZGSe at 2.6 eV and 1.75 eV, indicating the high solar absorbance capability of these materials in the visible region. The suitable band gap (1.59 eV) with high absorption coefficient of CZGSe produces significantly larger the current density and maximum upper limit of theoretical energy conversion efficiency ($P(\%)$) than that of CZGS. Overall, this comparative study enables us to understand the fundamental properties of these novel quaternary CZGS/Se chalcogenides for future solar harvesting applications.

ACKNOWLEDGMENTS

The work was supported by the Ministry of New and Renewable Energy (MNRE), Government of India, under the Grant No. 31/03/2014-15/PVSE-R&D. M.V.J. thank the supervisor Prof. Ranjit Thapa, Department of Physics, SRM University-AP, for his valuable discussions and suggestions. Author also would like to thank SRM Research Institute, SRM Institute of Science and Technology for providing computational facilities.

CONFLICT OF INTEREST

The author declare no conflicts of interest.

REFERENCES

1. C. Wang, S. Chen, J.H. Yang, L. Lang, H.J. Xiang, X.G. Gong, A. Walsh, and S.H. Wei, *Chem. Mater.* 26, 3411 (2014).
2. W. Wang, M.T. Winkler, O. Gunawan, T. Gokmen, T.K. Todorov, Y. Zhu, and D.B. Mitzi, *Adv. Energy Mater.* 4, 7 (2014).
3. H. Zhou, W.C. Hsu, H.S. Duan, B. Bob, W. Yang, T. Bin Song, C.J. Hsu, and Y. Yang, *Energy Environ. Sci.* 6, 2822 (2013).
4. M. Graetzel, R.A.J. Janssen, D.B. Mitzi, and E.H. Sargent, *Nature* 488, 304 (2012).
5. G.M. Ford, Q. Guo, R. Agrawal, and H.W. Hillhouse, *Chem. Mater.* 23, 2626 (2011).
6. S. Chen, A. Walsh, X.G. Gong, and S.H. Wei, *Adv. Mater.* 25, 1522 (2013).
7. S. Levcenco, D. Dumcenco, Y.S. Huang, K.K. Tiong, and C.H. Du, *Opt. Mater. (Amst).* 34, 183 (2011).
8. F. Hong, W. Lin, W. Meng, and Y. Yan, *Phys. Chem. Chem. Phys.* 18, 4828 (2016).
9. Z. Xiao, W. Meng, J.V. Li, and Y. Yan, *ACS Energy Lett.* 2, 29 (2017).
10. W. Shi, A.R. Khabibullin, and L.M. Woods, *Adv. Theory Simul.* 3, 2000041 (2020).
11. C.H.L. Goodman, *J. Phys. Chem. Solids* 6, 305 (1958).
12. B.R. Pamplin, *Nature* 188, 136 (1960).
13. A. Walsh, S. Chen, S.H. Wei, and X.G. Gong, *Adv. Energy Mater.* 2, 400 (2012).
14. S. Chen, X.G. Gong, A. Walsh, and S.H. Wei, *Phys. Rev. B Condens. Matter Mater. Phys.* 79, 165211 (2009).
15. J.S. Seol, S.Y. Lee, J.C. Lee, H.D. Nam, and K.H. Kim, *Sol. Energy Mater. Sol. Cells* 75, 155 (2003).
16. J.J. Scragg, P.J. Dale, and L.M. Peter, *Electrochem. Commun.* 10, 639 (2008).
17. M.I. Amal and K.H. Kim, *Chalcogenide Lett.* 9, 345 (2012).
18. K. Ito and T. Nakazawa, *Jpn. J. Appl. Phys.* 27, 2094 (1988).
19. W. Shi, A.R. Khabibullin, D. Hobbis, G.S. Nolas, and L.M. Woods, *J. Appl. Phys.* 125, 155101 (2019).
20. G.S. Nolas, M.S. Hassan, Y. Dong, and J. Martin, *J. Solid State Chem.* 242, 50 (2016).
21. G.E. Delgado, A.J. Mora, P. Grima-Gallardo, S. Duran, M. Munoz, and M. Quintero, *Cryst. Res. Technol.* 43, 783 (2008).
22. D. Hobbis, W. Shi, A. Popescu, K. Wei, R.E. Baumbach, H. Wang, L.M. Woods, and G.S. Nolas, *Dalton Trans.* 49, 2273 (2020).
23. S. Medina, K.O. Obodo, Y. Zaoui, H. Bendaoud, L. Beldi, and B. Bouhafs, *Comput. Condens. Matter* 23, e00459 (2020).
24. B.G. Yalcin, *Philos. Mag.* 96, 2280 (2016).
25. L. Bindi and J.A. Jaszczak, *Minerals* 10, 467 (2020).
26. G. Kresse and J. Hafner, *Phys. Rev. B* 48, 13115 (1993).
27. G. Kresse and J. Furthmuller, *Comput. Mater. Sci.* 6, 15 (1996).
28. G. Kresse and D. Joubert, *Phys. Rev. B Condens. Matter Mater. Phys.* 59, 1758 (1999).
29. J.P. Perdew, K. Burke, and M. Ernzerhof, *Phys. Rev. Lett.* 77, 3865 (1996).
30. H.J. Monkhorst and J.D. Pack, *Phys. Rev. B* 13, 5188 (1976).
31. A. Tkatchenko, L. Romaner, O.T. Hofmann, E. Zojer, C. Ambrosch-Draxl, and M. Scheffler, *MRS Bull.* 35, 435 (2010).
32. S. Kummel and L. Kronik, *Rev. Mod. Phys.* 80, 3 (2008).
33. S. Grimme, *Wiley Interdiscip. Rev. Comput. Mol. Sci.* 1, 211 (2011).
34. J. Klimes and A. Michaelides, *J. Chem. Phys.* 137, 120901 (2012).
35. E.R. Johnson, I.D. Mackie, and G.A. DiLabio, *J. Phys. Org. Chem.* 22, 1127 (2009).
36. K. Berland and P. Hyldgaard, *Phys. Rev. B Condens. Matter Mater. Phys.* 89, 035412 (2014).
37. J. Heyd, G.E. Scuseria, and M. Ernzerhof, *J. Chem. Phys.* 118, 8207 (2003).
38. J. Heyd and G.E. Scuseria, *J. Chem. Phys.* 120, 7274 (2004).
39. D.R. Penn, *Phys. Rev.* 128, 2093 (1962).